Pergamon

Geochimica et Cosmochimica Acta, Vol. 65, No. 19, pp. 3365–3377, 2001

0016-7037/01 $20.00 + .00

PII S0016-7037(01)00675-5

Cratonic peridotites and silica-rich melts: Diopside-enstatite relationships in polymict xenoliths, Kaapvaal, South Africa

HONGFU ZHANG,[1,2] MARTIN A. MENZIES,[2] JOHN J. GURNEY,[3] and XINHUA ZHOU[1]

[1]Laboratory of Lithosphere Tectonic Evolution, Institute of Geology and Geophysics, Chinese Academy of Sciences, P.O. Box 9825, Beijing 100029, P. R. China
[2]Department of Geology, Royal Holloway University of London, Egham, SurreyTW20 OEX, UK
[3]Department of Geochemistry, University of Cape Town, Cape Town, South Africa

(*Received April* 10, 2000; *accepted in revised form May* 5, 2001)

Abstract—Silica-rich metasomatism is invoked as a mechanism for the conversion of clinopyroxene-bearing peridotites to orthopyroxene-rich, clinopyroxene-poor peridotites. While harzburgites are a major constituent of the garnet–diamond facies "keel" of Archaean (> 2500 Ma) cratons, metasomatic conversion of lherzolite to harzburgite is not widely documented from cratonic rocks. We report on the replacement of diopside by enstatite in polymict peridotites from Kimberley, South Africa and provide elemental and isotopic constraints on the nature of this process. Silica-rich metasomatism appears to have occurred at mid-craton depths and to have involved a silica-rich derivative of incompatible element-rich melts like kimberlite. The preservation of elemental and isotopic disequilibria in these mantle rocks may arise from the nearly synchronous occurrences of the kimberlite entrainment process and fluid-assisted deformation/crack propagation resulting in polymict formation. *Copyright © 2001 Elsevier Science Ltd*

1. INTRODUCTION

Large degrees of partial melting of primitive mantle lherzolite is commonly proposed for the formation of residual mantle peridotites (harzburgite) that constitute the lowermost parts of the lithosphere within continental regions (Ringwood, 1958; Nixon and Boyd, 1973; Jordan, 1978; Hanson and Langmuir, 1978; Boyd, 1989; Walker et al., 1989; Walter, 1999; Herzberg, 1999). This model accounts for the depletion of basaltic components (FeO, TiO_2, CaO, Al_2O_3) in mantle rocks and can be used to constrain the depth of melting (Walter, 1999). However mantle peridotites from the Kaapvaal craton, South Africa are more orthopyroxene rich than one would expect from their composition and their proposed derivation by partial melting from a primitive mantle source rock (Herzberg, 1993). This has been variously attributed to their derivation as cumulate rocks with a mode determined by the proportion of cumulus olivine and intercumulus orthopyroxene (i.e., trapped melt) (Herzberg, 1993, 1999). A multistage melt infiltration model has been proposed as an alternative explanation for the formation of orthopyroxene-rich cratonic peridotites (e.g., Kelemen et al., 1992; Rudnick et al., 1994, Griffin et al., 1999). In this model, a melt residue was infiltrated by silica-rich fluids leading to loss of clinopyroxene and preferential growth of orthopyroxene, producing a rock much richer in silica than would be expected from a simple melting process. Thus, the high orthopyroxene mode/enriched silica content of the majority of low-temperature Kaapvaal peridotites is attributed to the interaction of silica-rich liquids with "normal" magnesian peridotites (i.e., 6–7 Gpa melt residues) (Walter, 1999). Such orthopyroxene-rich peridotites may have been produced during subduction-related accretion of continental material (e.g., Rudnick et al., 1994; Kelemen et al., 1998).

*Author to whom correspondence should be addressed (hfzhang@mail.igcas.ac.cn).

The theory that lherzolite (cpx bearing) was converted to harzburgite (opx rich) is partially supported by observations of natural peridotites and their constituent minerals. The involvement of metasomatic melts in peridotite transformation was first alluded to by Quick (1981) for the Phanerozoic Trinity orogenic massif, northern California. He described geologic relationships indicative of a replacive origin for the Trinity harzburgites because these rocks form sequential concentric zones around tabular dunites, which in turn, grade into spinel and plagioclase lherzolite. Contacts between the different zones were very sharp, a feature that was very difficult to explain by partial melting extraction models in a "normal" thermal gradient. Such marked discontinuities between distinct lithologies required reactive porous flow and as such, were direct geologic evidence for a metasomatic origin for the Trinity harzburgites. In the context of Archaean cratons, Griffin et al. (1999) used trace elements in zoned garnets from Wesselton, South Africa to demonstrate conversion of lherzolite to harzburgite. Rimward transformation of a Ca-saturated (lherzolitic) garnet precursor to a Ca-undersaturated (harzburgitic) garnet was interpreted as the result of the activity of metasomatic melt. Lherzolite to harzburgite transformation can also be inferred from replacement of diopside by enstatite in basalt-borne peridotite xenoliths from the Lashaine volcano, northern Tanzania (Dawson, 1987). In these rocks, the original clinopyroxene was partially or completely replaced by an aggregate of orthopyroxene with lesser amounts of chromite, phlogopite, and ilmenite.

In this paper we present elemental and isotopic data from a suite of polymict mantle xenoliths (JJG1414, BD2394, BD344) from the Kaapvaal craton, southern Africa. The main aims of the paper are to

1. Document the elemental and isotopic changes observed in orthopyroxene-clinopyroxene assemblages in polymict peridotites,
2. Constrain the P-T relationships using thermobarometry,

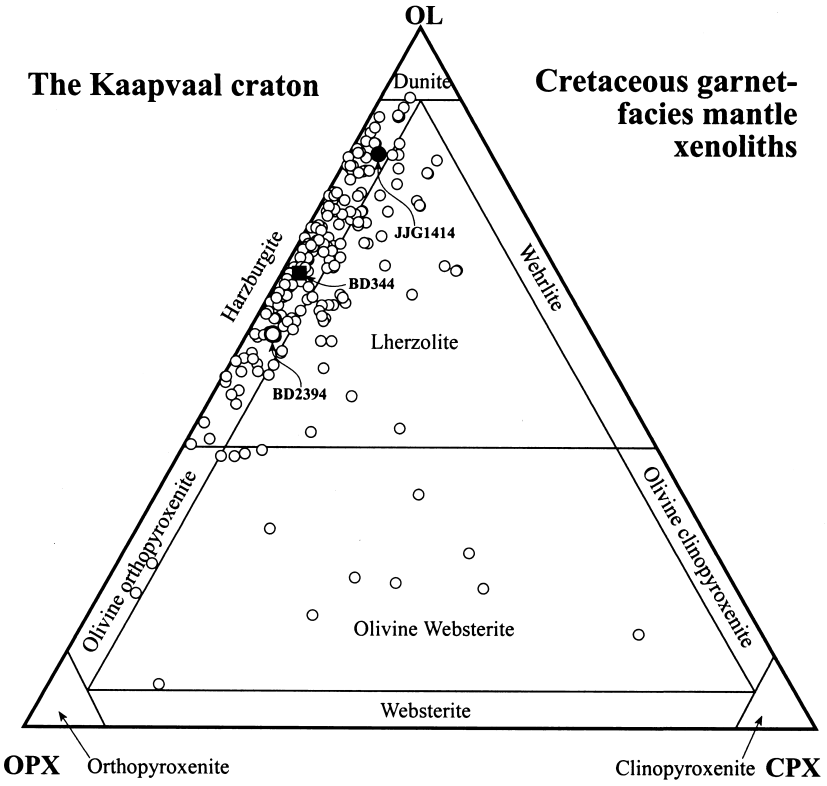

Fig. 1. Petrologic classification of the polymict xenoliths from Kimberley, South Africa. Solid circle, open circle, and filled square refer to sample JJG1414, BD2394, and BD344, respectively. Also shown are garnet-facies mantle xenoliths entrained in Cretaceous kimberlites from the Kaapvaal craton (i.e., open circles). Data compiled from Carswell and Dawson (1970), Mathias et al. (1970), Chen (1971), Maaloe and Aoki (1977), Boyd and Nixon (1978), Dawson (1990), Nixon (1987), Waters (1987), Walker et al. (1989), and Olive et al. (1997).

3. Calculate melt compositions using appropriate partition coefficients, and
4. Investigate the relevance of these data for the formation of off- and on-craton harzburgites by metasomatic processes.

2. PETROLOGY

Petrological descriptions of the polymict peridotites used in this study are given elsewhere (Lawless et al., 1979; Zhang, 1998; Morfi et al., 1999a,b; Zhang et al., 2000). The rocks contain garnet-bearing phases and can be termed "garnet harzburgites" (Fig. 1), but such a strict classification of these rocks may not apply because they have a very complex origin involving deformation and melt ingress (Zhang, 1998). Diopsides in the polymict xenoliths vary in grain size from 10 to 20 mm to $<$ 1 mm. They have a distinctive secondary enstatite rim, which partially or completely replaces the primary diopside (Fig. 2). The replacement is usually accompanied by the formation of finely disseminated ilmenite and rutile and in places is associated with the formation of garnet (JJG1414) and phlogopite (BD2394 and BD344) (Fig. 1). The grain boundaries between the diopside core and the enstatite rim are poorly defined and many are serrated with embayed edges. In many cases, rim enstatite is sheared to form a mosaic of subgrains, indicating that replacement predated deformation. Primary diopside replaced by phlogopite, secondary diopside, and enstatite has also been observed in a polymict xenolith. These textures may reflect diverse episodes of metasomatism that are different from those involved in the replacement of diopside by enstatite.

3. ANALYTICAL TECHNIQUES

3.1. Electron Microprobe

Major element compositions were obtained on double-polished graphite-coated slices with a JEOL Superprobe equipped with energy dispersive system and automation system (AN 10000/55S with 2500 CPS) at the Department of Geology, Birkbeck College, University of London. Analyses were performed with a beam of 15 KeV and 15 nA focused to a spot $\sim$1 μm in diameter. ZAF4 and Standard Cobalt were used for the online correction and spectrum calibration. Analytical precision was estimated with 0.5 wt.%.

3.2. Ion Microprobe

Trace element analysis was carried out in situ on double-polished, gold-coated slices with a Cameca ims-4f ion microprobe at the Department of Geology and Geophysics, Edinburgh University. It should be noted that to obtain enough intensity, acquisition time was increased to 15 s per cycle for elements with extremely low concentrations in the rim enstatites. The detailed measurement procedure is described elsewhere (Harte and Kirkley, 1997).

3.3. Laser Fluorination

Oxygen isotopes were analyzed using laser-fluorination techniques at the Department of Geology, Royal Holloway University of London. Core diopside and rim enstatite were carefully separated by handpick-

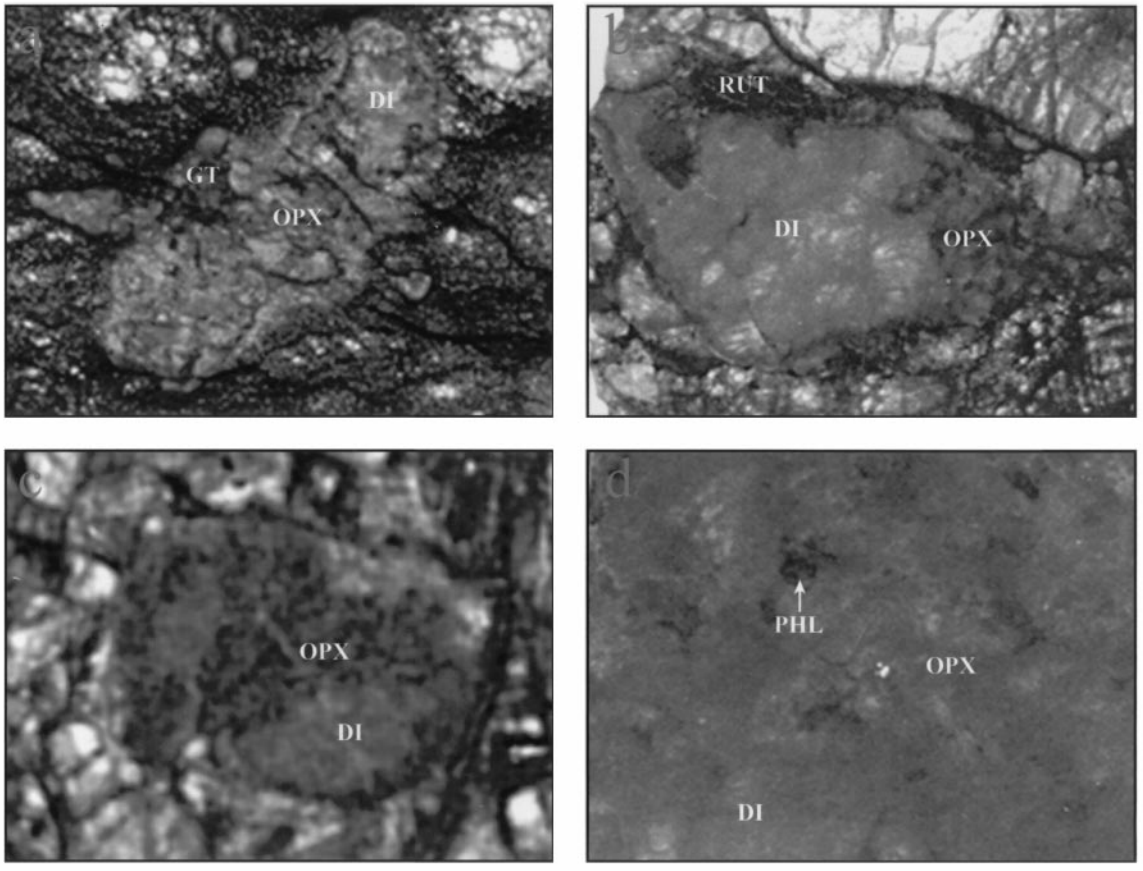

Fig. 2. Photograph of the polymict xenoliths (double-polished slice) from Kimberley, South Africa. Length of the field in (a) 1.5 cm, (b,c) 1.3 cm, and (d) 0.5 cm. (a) Diopside replaced by enstatite and accompanied by formation of garnet (JJG1414). (b) Diopside replaced by enstatite with a rutile outside the enstatite rim (BD344). (c) Diopside replaced by enstatite in BD2394. (d) Diopside replaced by enstatite and phlogopite in BD2394. Diopside, rim enstatite, garnet, phlogopite, and rutile are respectively abbreviated as DI, OPX, GT, PHL, and RUT.

ing under the binocular microscope and cleaned with acetone in an ultrasonic bath for more than 20 min. The weight of the minerals was normally between 1.4 and 1.6 mg. For small grain, the sample was mixed with another grain that had a similar major and trace element composition (i.e., diopside) or added to mineral whose oxygen isotope composition is already known (i.e., rim enstatite). In the latter case, the final isotope composition was calculated from the measured value. In this way, we could analyze almost all the grains of diopside and rim enstatite in the polymict peridotites, which provided the best opportunity to study oxygen isotope fractionation between diopside and rim enstatite during mineral transformation. The appropriate analytical method is described elsewhere (Zhang et al., 2000).

4. RESULTS

4.1. Major and Minor Elements

Electron and ion microprobe analyses of core diopside and rim enstatite from the polymict peridotites are given in Table 1. Core diopside from the polymict xenoliths has a uniform major element composition (SiO_2, CaO, Mg ratio) (Fig. 3) and is very similar to the diopside from garnet peridotites in Kaapvaal (Boyd and Nixon, 1978; Erlank et al., 1987) and garnet-free peridotites from Lashaine (Dawson, 1987). In contrast to the major elements, the diopside exhibits a large variation in minor elements (Cr_2O_3, Al_2O_3, TiO_2, Na_2O) (Fig. 3). Multiple analyses of several large grains demonstrate that inhomogeneity in minor elements exists between different grains but also between relicts of individual grains. Some diopside grains, especially in JJG1414, show higher FeO, Al_2O_3, TiO_2, and Na_2O at their bleached edges relative to central portions (Table 1). Compositional distinctions between samples are also apparent. The diopside from JJG1414 and from the Lashaine peridotites displays higher 100Mg/(Mg+Fe) (>90.6) and Cr_2O_3 (>1.2 wt.%) than the coarse counterparts from BD2394 and BD344, although both overlap in their oxide contents.

Rim enstatite has a distinctive composition compared to the associated diopside and "normal" (i.e., none-rim) enstatite from the same rock (Fig. 3). Relative to normal enstatite, rim enstatite is lower in SiO_2 and higher in Cr_2O_3, Al_2O_3, and CaO perhaps due to inherited characteristics from the primary diopside. Variation in the composition of secondary rim enstatite is also apparent between different rocks and within individual rocks. Rim enstatite (JJG1414) with higher Mg ratio, Cr_2O_3, Al_2O_3, and TiO_2 does not overlap in composition with normal enstatite. In contrast, rim enstatite (BD2394 and BD344) is low in Mg ratio, Cr_2O_3, Al_2O_3, and TiO_2 (Fig. 3), except for one

Table 1. Representative elemental and oxygen isotopic compositions in diopsides and rim enstatites from Kimberley polymict peridotites, South Africa.

Sample	BD344		BD2394								JJG1414										
Grain			Grain 1			Grain 2		Grain 3			Grain 1			Grain 2		Grain 3		Grain 4		Grain 5	
Mineral	DI	EN	D1					DI			DI										
			Centre	Edge	EN	DI	EN	Centre	Edge	EN	Centre	Edge	EN	DI	EN	DI	EN	DI	EN	DI	EN
Major element compositions (Electron microprobe, wt%)																					
SiO_2	55.10	57.78	55.64	55.23	58.00	55.17	57.22	55.45	-	57.45	54.81	54.76	56.76	54.95	57.07	54.73	59.15	54.63	57.48	55.13	56.76
TiO_2	0.34	0.07	0.37	0.30	0.23	0.47	0.25	0.37	-	0.29	0.39	0.51	0.35	0.41	0.29	0.44	0.12	0.32	0.25	0.44	0.17
Al_2O_3	1.51	0.62	1.04	0.97	0.79	2.77	1.75	1.95	-	0.95	1.35	1.78	1.67	1.82	1.85	2.27	0.85	1.72	1.71	1.96	2.96
Cr_2O_3	0.91	0.50	0.80	0.75	0.32	1.61	0.93	1.01	-	0.63	2.08	2.11	1.33	2.57	1.02	2.63	0.41	2.60	1.45	2.54	1.27
FeO	3.06	7.68	3.20	3.19	7.41	3.15	6.86	3.41	-	7.22	2.94	3.17	5.63	2.57	5.32	2.70	4.56	2.41	5.94	2.62	5.34
MnO	0.05	0.11	0.08	0.12	0.12	0.10	0.25	0.08	-	0.23	0.04	0.03	0.04	0.04	0.11	0.03	0.06	0.13	0.20	0.03	0.02
MgO	15.86	31.74	15.83	15.84	32.11	15.07	31.41	15.38	-	31.68	16.50	16.97	32.40	15.86	32.66	16.20	34.33	15.81	31.85	15.68	31.78
CaO	21.52	1.03	22.06	22.20	0.76	18.73	0.88	20.38	-	0.68	19.87	18.66	1.14	19.17	0.92	18.41	0.54	19.80	1.31	19.20	1.14
Na_2O	1.73	0.43	1.63	1.60	0.54	2.79	0.46	2.38	-	0.44	1.99	2.13	0.65	2.57	0.56	2.53	0.31	2.61	0.57	2.55	0.48
Total	100.10	99.96	100.65	100.20	100.28	99.84	100.01	100.41	-	99.57	99.97	100.12	99.97	99.93	99.80	99.94	100.31	100.03	100.76	100.15	99.92
Trace element abundances (Ion microprobe, ppm)																					
Sr	131	0.56	112	132	14.1	83	0.32	108	126	4.56	141	175	4.94	117	2.33	132	1.19	181	2.90	138	0.57
Y	4.7	0.12	4.7	4.8	0.41	3.8	0.14	4.8	4.8	0.18	3.4	3.7	0.25	3.4	0.22	4.7	0.18	3.8	0.21	3.7	0.16
Zr	93	2.59	121	124	7.18	66	2.40	117	124	3.15	63	67	2.07	46	1.94	63	1.32	42	2.15	51	1.97
Hf	5.47	0.22	6.84	7.71	0.39	3.96	0.11	6.92	7.05	0.18	2.51	3.33	0.11	2.20	0.07	2.80	0.10	2.94	0.15	2.71	0.07
Nb	0.39	0.16	0.36	1.35	1.16	1.25	0.05	0.43	2.11	0.68	0.63	2.23	0.31	0.67	0.22	1.83	0.09	0.58	0.28	1.40	0.13
Ba	0.29	0.14	0.27	6.98	6.18	4.15	0.03	0.47	116	0.53	0.20	19.1	2.55	0.32	1.90	59.1	0.21	0.10	1.24	8.20	0.47
La	2.59	0.04	2.30	3.07	0.99	1.78	0.008	2.00	3.96	0.36	2.19	4.47	0.28	1.63	0.19	7.15	0.018	2.03	0.31	2.32	0.01
Ce	10.83	0.12	9.88	11.80	2.25	5.93	0.034	8.57	12.10	0.57	8.55	13.50	0.59	6.60	0.43	18.90	0.063	8.31	0.79	8.73	0.05
Pr	2.12	0.02	1.94	2.10	0.27	1.02	0.006	1.60	1.95	0.06	1.71	2.38	0.08	1.28	0.05	2.70	0.011	1.69	0.12	1.54	0.01
Nd	12.37	0.12	11.50	12.50	1.11	5.98	0.052	9.29	10.59	0.24	10.10	14.00	0.35	7.67	0.23	12.60	0.068	10.45	0.54	9.26	0.07
Sm	3.24	0.05	3.14	2.93	0.24	1.72	0.020	2.47	2.79	0.07	2.07	3.26	0.09	2.06	0.05	3.21	0.032	2.71	0.12	2.58	0.03
Eu	1.04	0.020	0.97	0.92	0.070	0.54	0.008	0.78	0.84	0.022	0.80	0.86	0.03	0.65	0.017	0.96	0.014	0.72	0.029	0.70	0.012
Gd	2.80	0.074	2.85	2.60	0.198	1.63	0.043	2.31	2.26	0.067	2.06	2.24	0.080	1.67	0.046	2.53	0.057	2.11	0.063	1.92	0.036
Tb	0.34	0.013	0.30	0.30	0.030	0.23	0.009	0.32	0.32	0.012	0.24	0.26	0.009	0.22	0.006	0.35	0.012	0.25	0.008	0.23	0.006
Dy	1.62	0.087	1.55	1.53	0.170	1.26	0.071	1.48	1.52	0.080	1.08	1.02	0.039	0.95	0.046	1.67	0.107	1.20	0.035	1.09	0.036
Ho	0.23	0.023	0.20	0.18	0.029	0.18	0.017	0.24	0.22	0.016	0.16	0.18	0.005	0.14	0.008	0.23	0.027	0.17	0.006	0.18	0.007
Er	0.48	0.062	0.38	0.40	0.072	0.36	0.071	0.49	0.43	0.044	0.40	0.45	0.010	0.27	0.026	0.51	0.088	0.30	0.015	0.31	0.016
Tm	0.06	0.011	0.04	0.05	0.009	0.05	0.012	0.06	0.05	0.006	0.04	0.05	0.001	0.03	0.003	0.05	0.018	0.03	0.002	0.03	0.002
Yb	0.34	0.088	0.24	0.25	0.047	0.27	0.086	0.34	0.29	0.040	0.24	0.29	0.004	0.17	0.019	0.23	0.158	0.17	0.013	0.16	0.010
Lu	0.04	0.013	0.03	0.03	0.006	0.03	0.019	0.04	0.04	0.006	0.03	0.03	0.000	0.02	0.002	0.02	0.026	0.02	0.002	0.02	0.001
Oxygen isotopes (Laser fluorination %)																					
$\delta^{18}O$	5.42	4.73	5.04	-	5.13	5.05	5.01	5.15	-	4.57	5.27	-	5.44	5.24	5.38	5.60	5.34	5.40	4.84	5.17	5.64

Table 2. Equilibrated temperatures and pressures when the replacement of diopside by enstatite happened.

			BD2394				JJG1414					
			Grain 1				Grain 1					
Sample		BD344	Core	Edge	Grain 2	Grain 3	Core	Edge	Grain 2	Grain 3	Grain 4	Grain 5
Cpx	X_{EN}	0.540	0.527	0.525	0.595	0.559	0.591	0.612	0.618	0.630	0.633	0.613
	X_{WO}	0.416	0.422	0.437	0.350	0.400	0.373	0.350	0.354	0.335	0.313	0.346
Opx	X_{EN}	0.863	0.872	0.872	0.875	0.875	0.890	0.890	0.900	0.921	0.882	0.893
	X_{WO}	0.020	0.015	0.015	0.018	0.013	0.023	0.023	0.018	0.010	0.026	0.023
T (Cpx + Opx)		1073 ± 116	1031 ± 39	999 ± 91	1116 ± 98	1022 ± 118	1156 ± 158	1175 ± 167	1117 ± 220	1039 ± 99	1232 ± 114	1192 ± 131
T (Cpx + X_{WO})		1125 ± 6	1045 ± 14	1043 ± 2	1129 ± 51	1056 ± 42	1197 ± 34	1206 ± 43	1160 ± 51	1033 ± 71	1239 ± 43	1210 ± 42
Err $X_{EN\ in\ Opx}$		+4.87%	+1.83%	+4.36%	+3.31%	+5.69%	+3.93%	+3.93%	+4.67%	+2.17%	+2.27%	+3.02%
T (Opx + X_{WO})		1099 ± 1	1035 ± 12	1019 ± 8	1110 ± 49	1030 ± 37	1176 ± 31	1184 ± 40	1133 ± 48	1020 ± 71	1224 ± 42	1194 ± 40
Err $X_{EN\ in\ Cpx}$		−4.07%	−1.52%	−3.24%	−3.03%	−3.76%	−3.72%	−3.76%	−4.53%	−2.22%	−2.84%	−3.10%
T (°C)		1112	1040	1031	1120	1043	1186	1195	1147	1027	1231	1202
P_{BK} (Kb)		24.4		25.0	34.4	31.7		34.2	37.6	40.8	34.3	36.6

Temperatures were calculated on the basis of two-pyroxene thermometer at the fixed pressure of 30 kbar by using QUILF program (Andersen et al., 1993) and all four reactions are used in these T estimations. T (Cpx + Opx) indicates that the calculation was taken by using all the measured cpx (i.e., augite) and opx compositions. The uncertainty is not a statistical uncertainty and refers only to the consistency of the least-squares fit between the solvus and Mg-Fe-Ca exchange. If taking the cpx composition and the X_{wo} of opx (i.e., letting the X_{EN} of opx float) we get T (Cpx + X_{wo}). Err $X_{EN\ in\ Opx}$ represents the percentage of differences between the best-fit calculated value and the measured value and can be expressed by $(X_{EN\ calculated}-X_{EN\ measured})/X_{EN\ measured}$. Similarly, if taking the opx composition and the X_{wo} of cpx (i.e., letting the X_{EN} of cpx float) we get T (Opx + X_{wo}) and Err $X_{EN\ in\ Cpx}$. T (°C) indicates the best approximation. P_{BK} is Al in opx barometer at the known temperature (Brey and Köhler, 1990).

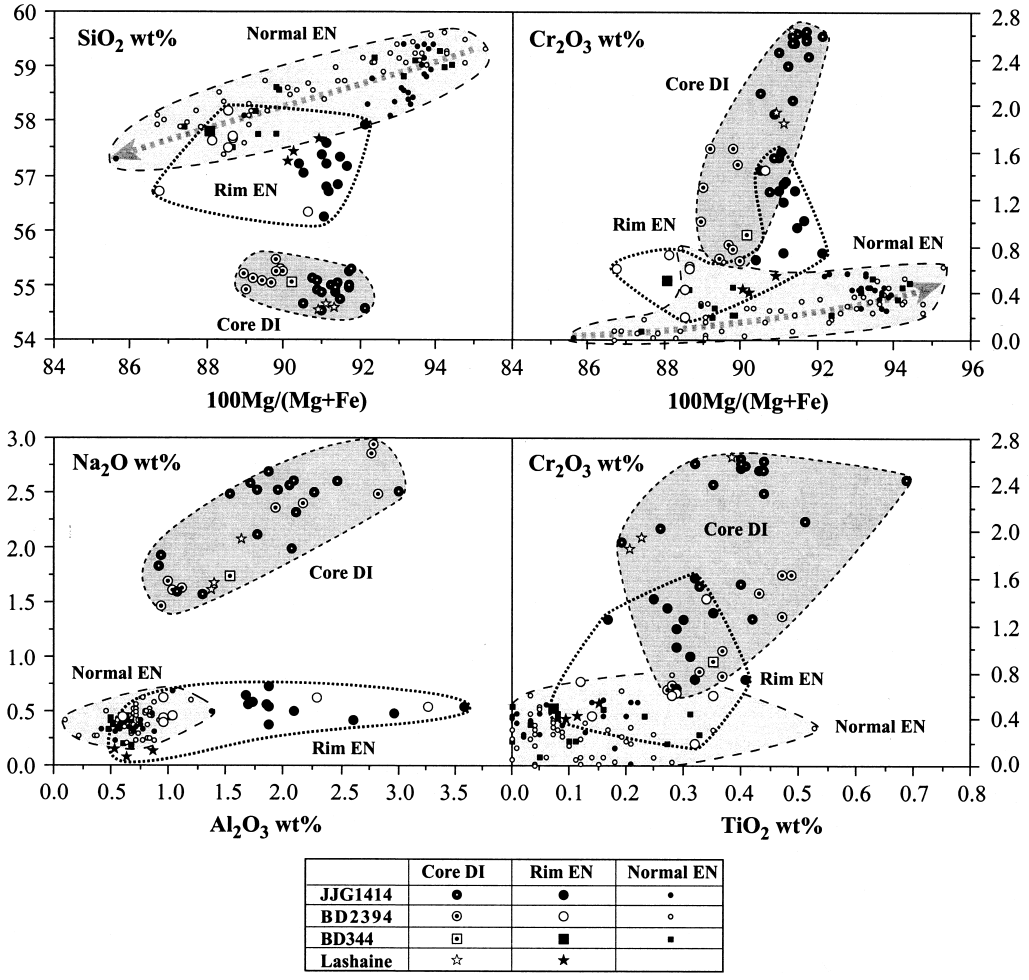

Fig. 3. Major and minor element variations in rim enstatite from Kimberley polymict peridotites, compared with core diopside and "normal" enstatite. Oxide plots as weight percentage after recalculation to 100%. 100 Mg/(Mg+Fe) is the atomic ratio. Lashaine lherzolite (BD1544 and BD3929) is from northern Tanzania (Dawson, 1987). Core DI = centre of diopside replaced by enstatite; Rim EN = rim enstatite on diopside; Normal EN = enstatite.

analysis which falls within the compositional field of JJG1414. Rim enstatite overlaps with normal enstatite and partially shows some similarities to normal enstatite and the rim enstatite from Lashaine. Moreover, elemental distribution within a single grain is highly variable and depends on the degree of replacement and the composition of the associated diopside. The maximum variation within an individual grain is ± 0.11wt.% TiO_2, ± 1.16wt.% Al_2O_3, ± 0.42wt.% Cr_2O_3, and ± 0.19wt.% CaO. This may indicate that full elemental equilibrium was not attained during the replacement of primary diopside by secondary enstatite.

4.2. Trace Elements

All the diopside grains from polymict xenoliths have similar LREE-enriched chondrite-normalised REE patterns with a Nd maximum (Fig. 4). This convex-upward REE pattern is typical of diopside from garnet-facies mantle xenoliths (e.g., Ehrenberg, 1982; Kramers et al., 1983; Menzies et al., 1987). Relative to the core composition, diopside close to a rim of secondary enstatite exhibits more LREE enrichment (Fig. 4) and higher trace element concentrations (e.g., Sr, Nb, Hf, Y) (Table 1). Despite this, all the diopsides show relatively constant Zr/Hf. Again, such a trace-element characteristic may indicate that trace-element equilibrium was not reached during metasomatism.

In contrast to the relatively uniform composition of the core diopside, the rim enstatite displays a large variation in trace element concentration (Table 1; Figs. 4, 5). Two types of chondrite-normalised REE patterns exist:

LREE-enriched rim enstatite ($(Ce/Yb)_N$ = 3.8 to 40) (JJG1414 and BD2394) and

LREE-depleted rim enstatite ($(Ce/Yb)_N$ = 0.11 to 0.37) (JJG1414, BD2394, and BD344)

One rim enstatite (JJG1414) has a unique MREE-enriched REE profile, lying between LREE-enriched and LREE-depleted. Total REE abundance correlates with the degree of LREE enrichment (Fig. 5) and with other elemental abundance. This is

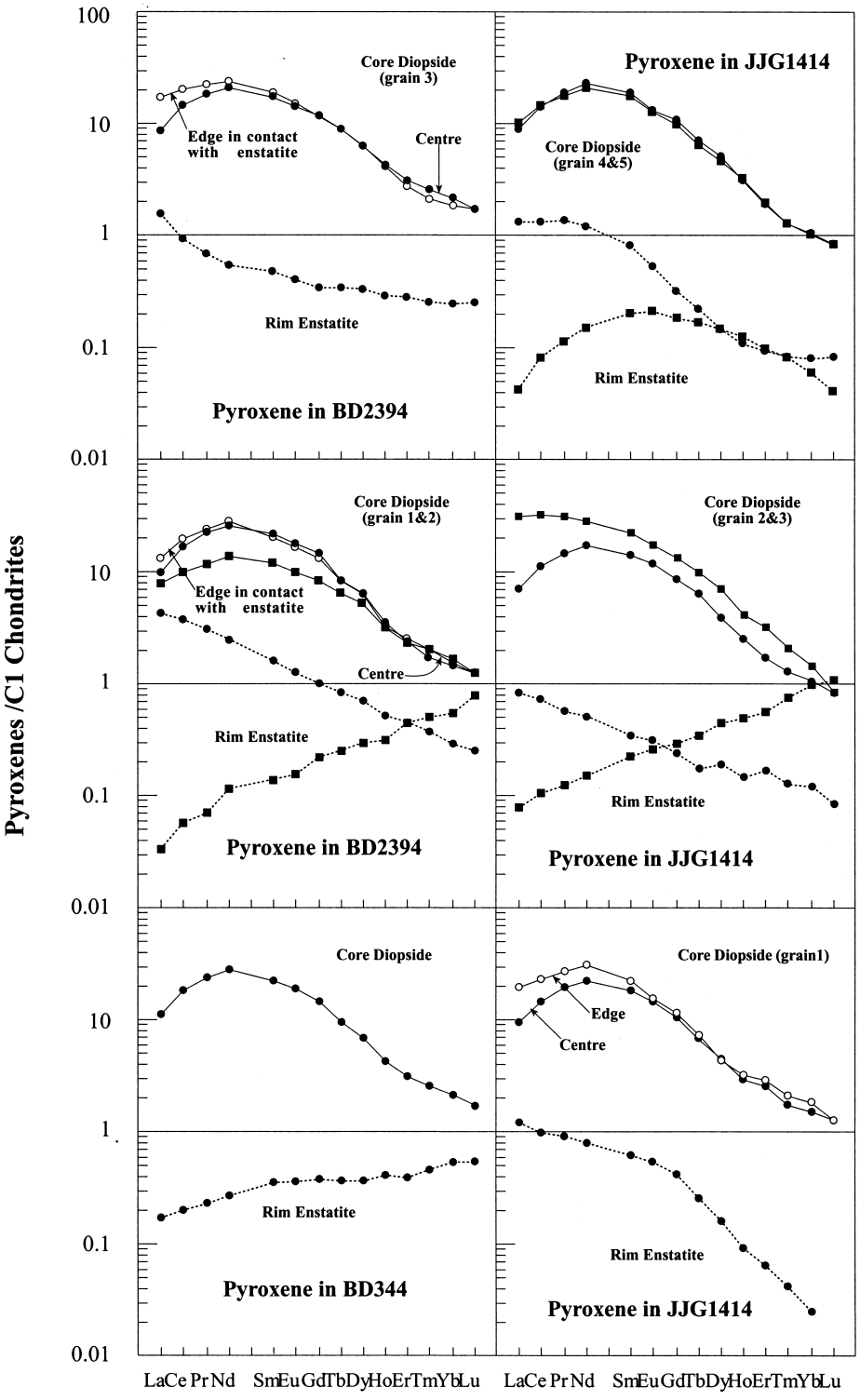

Fig. 4. Chondrite-normalised REE patterns of core diopsides and rim enstatites in Kimberley polymict peridotites, South Africa. Solid line and dotted line with the same symbol (i.e., solid circle or square) represent core diopside and rim enstatite, respectively (Table 1). Open circle indicates that the diopside is in contact with enstatite. Normal enstatite had extremely low trace element concentration below the detection limit of the SIMS (Cameca[@] ims-4f). C1 chondrite values are from Anders and Grevesse (1989).

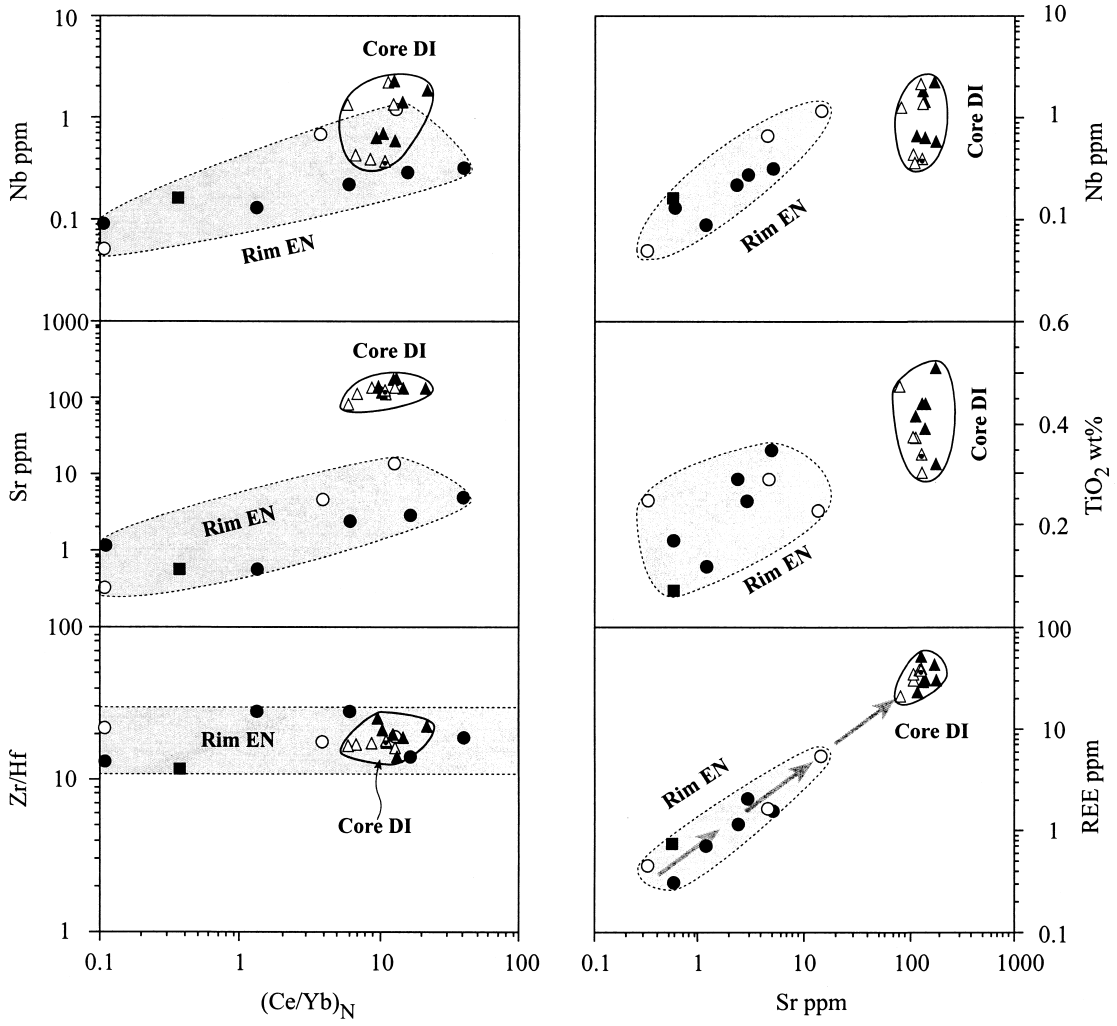

Fig. 5. Variations in trace element abundances of diopsides and enstatites from Kimberley polymict xenoliths, South Africa. Key as in Figure 3. Solid triangle, open triangle, and open triangle with a dot inside, respectively, refer to diopside in JJG1414, BD2394, and BD344.

particularly true for Sr. The excellent positive correlation between REE and Sr in rim enstatite indicates that the REE enrichment was accompanied by an increase in Sr with the maximum value recorded close to the diopside. In addition, other trace elements (i.e., Nb, Sr, Ti) positively correlate with $(Ce/Yb)_N$ and/or Sr. A reasonable conclusion is that the rim enstatite was formed by metasomatism and that the metasomatic melt responsible for the replacement of diopside by enstatite was enriched in Sr, Nb, Ti, Y, and the LREE.

4.3. Oxygen Isotopes

Diopside in the polymict harzburgite has a very uniform oxygen isotope composition except for JJG1414 (Zhang et al., 2000). The oxygen isotope value for the polymict peridotite is lower than the average for diopside from garnet-facies mantle peridotite worldwide (Fig. 6), but oxygen isotope data for JJG1414 and BD344 overlap with oxygen isotope data for garnet-facies mantle xenoliths from around the world. Correspondingly, the rim enstatite displays an extremely low oxygen isotope ratio, much lower than the coexisting normal enstatite and that from garnet-facies mantle xenoliths worldwide (Fig. 6). The only overlap in oxygen isotope ratio between rim enstatite and normal enstatite was found in JJG1414. The large variability in oxygen isotopes in rim enstatite, relative to core diopside, may indicate that oxygen isotope equilibrium was not reached during metasomatism. The low oxygen isotope composition in rim enstatite and core diopside may illustrate that the metasomatic melt had a low oxygen isotope composition. Another unique feature is that oxygen isotope fractionation between the primary core diopside and the secondary rim enstatite plots outside the well-documented field for mantle peridotites (Fig. 7).

5. DISCUSSION

5.1. Ca vs. Si-rich Metasomatism

Two types of metasomatism have been reported from cratonic mantle peridotites: Ca and Si metasomatism.

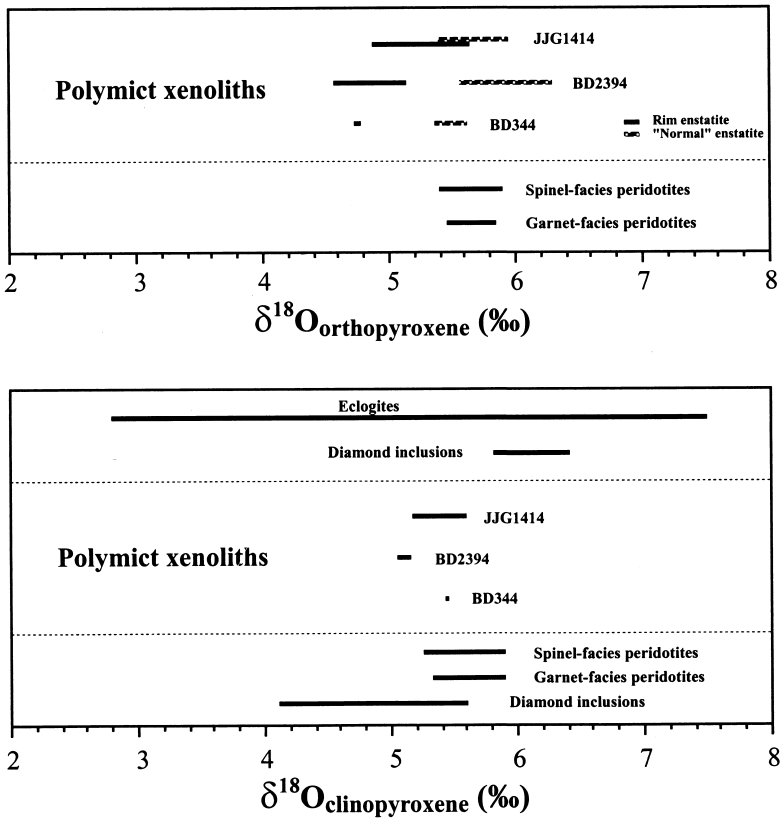

Fig. 6. Oxygen isotope compositions in enstatites (top figure) and diopsides (bottom figure) from the Kimberley polymict xenoliths, South Africa, compared with those from P-type diamond inclusions and peridotites and with E-type diamond inclusions and eclogites. Oxygen isotopes of minerals from P-type and E-type diamond inclusions and peridotites and eclogites are from Mattey et al. (1994a,b), Lowry et al. (1993, 1994), Xu et al. (1996), and Chazot et al. (1997).

Ca metasomatism is characteristic of cratonic peridotite and evident as the replacement of orthopyroxene by clinopyroxene and of olivine by monticellite. Secondary diopside as a rim and overgrowth has been reported from the Siberian craton, Russia (Boyd et al., 1997), the Kaapvaal craton, South Africa (Erlank et al., 1987; Boyd et al., 1997), and the Slave craton, Canada (Boyd and Canil, 1997; MacKenzie and Canil, 1999). Zoned garnet in low-Ca harzburgite points to the transformation of Ca-poor garnet to Ca-rich garnet due to the action of melt (Schulze, 1991; Boyd et al., 1993; Griffin et al., 1999). This indicates a process distinct to that found in the polymict peridotite. The formation of Ca-rich phases leads to the conversion of harzburgite (Ca poor) to lherzolite (Ca rich) and is the opposite process to what is observed in the polymict peridotites.

Si metasomatism is a characteristic of polymict xenoliths where silica addition leads to orthopyroxene precipitation and the dissolution of olivine and clinopyroxene. Indirect evidence of silica metasomatism comes from mass balance calculations and experimental data (Walter, 1998). Kelemen et al. (1992, 1998) used these data to demonstrate that the average mantle xenolith composition from the Kaapvaal and Siberian cratons could not be a simple residue of partial melting. Residues formed by partial melting of primitive mantle at pressures of 25 to 140 kbar cannot have more than 23% orthopyroxene, but orthopyroxene modes of 30% and higher are known for spinel-

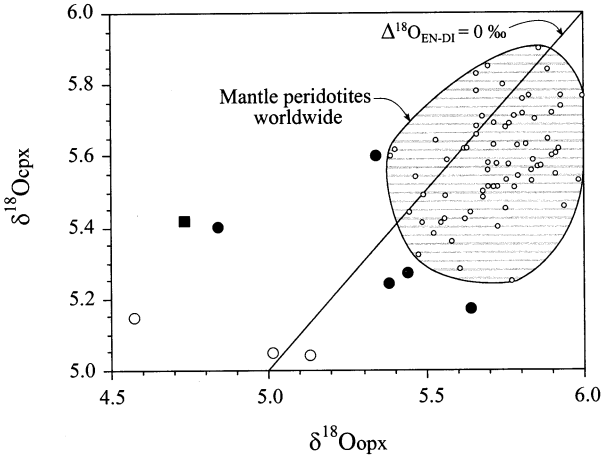

Fig. 7. Oxygen isotope fractionation between core diopside and rim enstatite from the polymict xenoliths, South Africa. The mantle peridotite field includes minerals from P-type diamond inclusions, garnet-facies, and spinel-facies mantle peridotites worldwide (Mattey et al., 1994a,b; Lowry et al., 1993, 1994; Xu et al., 1996; Chazot et al., 1997). The equilibrated oxygen isotope fractionation between enstatite and diopside in normal mantle rocks is $< 0.3‰$. Solid circle, open circle, and filled square refer to samples JJG1414, BD2394, and BD344, respectively; small-open circle indicates the comparative data of worldwide mantle peridotites in the literature.

and garnet-facies peridotites from Kaapvaal and Siberia. To explain this anomaly, several authors (e.g., Rudnick et al., 1994; Kelemen et al., 1992, 1998) argued that orthopyroxene-rich mantle peridotites were modified by the addition of a small amount of silica-rich melt and thus requires at least a two-stage process. The first stage sees the creation of high Mg#, low orthopyroxene peridotites by a large degree of polybaric decompression melting. Later, these depleted residues are enriched in orthopyroxene by interaction with silica-rich melts generated mainly by partial melting of subducted metabasalts or metasediments. This melt influx triggers the dissolution of olivine and clinopyroxene and the precipitation of orthopyroxene. This model accounts for both the magnesium and silica-rich nature of many cratonic peridotites and the correlation of Ni in olivine vs. mode of orthopyroxene in cratonic harzburgites (e.g., Kelemen et al., 1998). Thus, at least half of the Kaapvaal and Siberia harzburgite xenoliths must have been modified by an influx of silica-rich melt (Kelemen et al., 1998; Canil, 1992). As such the silica metasomatism is important in our understanding of craton evolution and the timing of both Ca and Si-rich metasomatic processes holds vital clues as to how cratons form. The preservation of elemental and oxygen isotopic disequilibria indicates that the process of Si metasomatism preserved in the Kaapvaal xenoliths was "young" and presumably must have been synchronous with entrainment of the xenoliths for these disequilibria to be frozen in time. A longer period of time at higher elevated temperatures would have obliterated such rare disequilibria. The textural relationships indicate that silica metasomatism predated deformation, perhaps indicating that melt ingress made the rock more susceptible to deformation. In summary, Si metasomatism in cratonic peridotites may have been as widespread as Ca metasomatism, but the petrological evidence for Si metasomatism is rare in the rock record because in many cases, deformation may have completely destroyed these textures.

5.2. Polymict Peridotites: Lherzolite or Harzburgite Protolith?

Polymict rock JJG1414 contains more than 5% diopside, so one could argue that the protolith was lherzolite. Furthermore, the Cr_2O_3 and CaO contents of the majority of garnets from polymict peridotites (Zhang, 1998) plot within the "lherzolite field" (Meyer, 1987) rather than the "harzburgite field." Two high-CaO garnets that plot outside the lherzolite field may be anomalous, i.e., water-bearing garnet (JJG1414) (Zhang, 1998). However, elemental and oxygen isotope data indicate a complex origin resulting in the juxtaposition of minerals of diverse provenance possibly in an environment of fluid-assisted deformation. Although a mode as such may be meaningless in determining the premetasomatic protolith type (Zhang et al., 2000), silica-rich metasomatism is a process that alters a lherzolite precursor to harzburgite. This metasomatism results in (a) inter- and intra-mineral elemental and oxygen isotope disequilibrium (Zhang et al., 2000), (b) the LREE and LILE enrichment, and (c) ^{18}O depletion in rim enstatite and diopside. Therefore, the replacement mechanism may be related to a metasomatic episode that converted lherzolite protoliths to orthopyroxene-rich harzburgites (e.g., JJG1414, BD2394, and BD344) or clinopyroxene-free harzburgite (BD2666).

5.3. Thermobarometry

Equilibration temperature for the two-pyroxene assemblages was calculated using the program QUILF (Anderson et al., 1993). The QUILF program provides three ways of calculating the equilibration temperature for a two-pyroxene assemblage. One way is to use the compositions of both pyroxenes, in which case the program calculates the best fit to both the solvus thermometer and the Fe-Mg exchange. The other way is to calculate the temperature as defined by the solvus thermometer using the composition of either the Opx or Augite (see also Frost and Lindsley 1992). It is obvious from Table 2 that the temperature calculated using the compositions of both the pyroxenes, i.e., T(Clinopyroxene + Orthopyroxene), is similar (though with a greater uncertainty of course) to those obtained when the composition of one pyroxene is allowed to vary, i.e., T(Clinopyroxene + XWo) and T(Orthopyroxene + XWo). From these calculations, it appears that replacement of diopside by enstatite in polymict xenoliths occurred around 1000 to 1200°C with a hint of higher temperatures in the deformed xenoliths. Observations of higher temperatures in sheared xenoliths and lower ones in granular xenoliths have been reported elsewhere (Finnerty and Boyd, 1987, and references therein).

With temperatures constrained, we can calculate the equilibrated pressure by using Al in an orthopyroxene barometer (Brey and Köhler, 1990). The determination of the temperature and the pressure at which mantle processes operated (Brey and Köhler, 1990; Jones and McKay, 1992; Kelemen et al., 1993; Johnson, 1998; Eggins et al., 1998; Schwandt and McKay, 1998) is pivotal to understanding lithosphere evolution, but it must be stressed that the complex nature of these rocks means that juxtaposition of minerals does not imply that they are cogenetic or in equilibrium. The extent of oxygen isotope disequilibrium and the correlation between oxygen isotopes and elemental concentrations (Zhang et al., 2000) emphasize the lack of complete equilibration. It is the existence of such an incomplete equilibration that led to the occurrence of a wide range of pressures in a single rock. Since these calculations reveal that the metasomatic processes occurred at 25 to 37 kb (i.e., 80–124 km), the range probably reflects more about the complex genesis of the rocks than any other factor. Overall, these calculations are consistent with the polymict rocks having formed at midcraton depths (i.e., garnet facies mantle) within the Archaean lithosphere, since the craton is estimated to have been >200km thick at the time of entrainment (Boyd et al., 1985). Midcraton depths are associated with intense metasomatism at levels of 75 to 100 km (Haggerty 1989a,b) mainly because of the shape of the C-H-O solidus closer to upwelling melt to freeze within the mantle. Two metasome horizons are believed to develop at 50 to 75 km and 75 to 100 km, the latter being of interest in the formation of the polymict rocks.

5.4. Infiltrated Melt Compositions

The systematic elemental and isotopic variations (Figs. 3, 5, 6) in secondary rim enstatite relative to primary core diopside and/or "normal" enstatite illustrate that the conversion of original diopside to enstatite, ilmenite, rutile assemblages requires

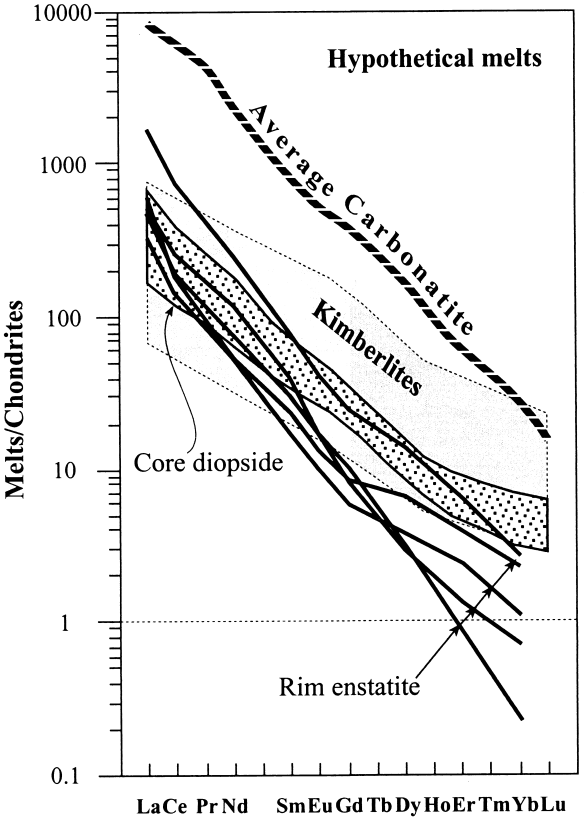

Fig. 8. Hypothetical melt composition in equilibrium with core diopside and LREE-enriched rim enstatite from Kimberley polymict xenoliths. The mineral-melt partition coefficients are from Foley et al. (1994) and Kelemen et al. (1990). The shaded field represents the compositional ranges of kimberlites (Muramatsu, 1983; Mitchell, 1986; Erlank et al., 1987; Dawson, 1990). The average carbonatite is recalculated from the original data of Nelson et al. (1988) and Woolley and Kempe (1989).

the addition of Si, Ti, Fe, LREE, etc. from metasomatic melts and the concomitant removal of Ca and Na.

The metasomatic melts must have been enriched in Si, LREE, Nb, Sr, Ti, Fe, and Cr and poor in ^{18}O, similar to the infiltrating melt involved in the formation of ilmenite-rutile-phlogopite-sulphide veins in mantle peridotites (Harte et al., 1987). The development of enstatite rather than amphibole suggests that the fluid was low in H_2O, or that the replacement took place perhaps at greater depths or higher temperatures, outside the stability field of amphibole (Dawson, 1987). The composition of the hypothetical melt can be calculated using pyroxene/melt partition coefficients. These have been shown to be a function of temperature and pressure and pyroxene compositions (Jones and McKay, 1992; Kelemen et al., 1993; Johnson, 1998; Eggins et al., 1998; Schwandt and McKay, 1998). The REE partition coefficients of Foley et al. (1994) were selected for typical diopside. Recent experimental studies of clinopyroxene (Johnson, 1998) showed that trace-element partitioning is not a strong function of T and P, except for Ti, which displays a mild T dependence. The calculated hypothetical melts for all core diopsides (Fig. 8) fall within the compositional ranges of global kimberlites (e.g., Muramatsu, 1983; Mitchell, 1986; Erlank et al., 1987; Dawson, 1990), probably illustrating that the melt composition involved in diopside formation had a kimberlitic character. For rim enstatite, proper selection of REE partition coefficients is more difficult because partitioning is strongly dependent on Al and Ca contents of the orthopyroxene (Jones and McKay, 1992; Schwandt and McKay, 1998) as well as ambient T and P (Eggins et al., 1998). A set of REE partition coefficients compiled by Kelemen et al. (1990) were used to infer melt composition. The hypothetical melts calculated from LREE-enriched rim enstatites (Fig. 8) have chondrite-normalised REE abundances consistent with that displayed by global kimberlites except for the HREE abundances, which are much lower than kimberlites. If one takes more recently published data (Kelemen et al., 1993; Schwandt and McKay, 1998), the hypothetical melts calculated from LREE-enriched rim enstatites tend to be similar to average carbonatite. This may indicate that replacement of diopside by rim enstatite in Kimberley polymict xenoliths happened in the presence of carbonatitic melts. The suggestion that the formation of polymict peridotites may have involved kimberlitic or carbonatitic melts is of interest because the metasome horizons in the lithosphere (Haggerty, 1989a,b) are repositories for both melt compositions. The shallow metasome is associated with carbonatitic trace element characteristics (50–75 km) and the deeper metasome with kimberlitic trace element characteristics (75–100 km). The deeper metasome is also believed to be potassium and water rich, consistent with inferences based on the geochemistry of the polymict rocks (Zhang, 1998). Bearing in mind that kimberlites are in themselves polymict melts, one could speculate that the polymict mantle rocks may represent frozen kimberlites.

6. CONCLUSIONS

Metasomatic replacement of diopside by enstatite in polymict xenoliths records only part of a very complex petrogenetic history. Metasomatic melt processes are believed to be inextricably linked to deformation and possibly represent crack propagation fueled by the transfer of silicate melts through the lithosphere. The nearly synchronous occurrence of these processes may account for elemental and oxygen isotopic disequilibrium, isotope-elemental and isotope-grain size correlations. In other words, kimberlite entrainment has captured short-lived, and somewhat rarely preserved, isotope and elemental disequilibria. Zhang et al. (2000) suggested that the polymict peridotites were sites of preferential deformation and melt percolation and that relative movement/transport along mantle shear zones had led to the juxtaposition of minerals of varied provenance.

Pervasive reaction between peridotite protoliths and ascending melts with concomitant dissolution of calcium-pyroxene and precipitation of orthopyroxene is repeatedly invoked as a major shallow mantle process (e.g., Kelemen et al., 1992; Rudnick et al., 1994, Kelemen et al., 1998). However, limited petrological evidence of such a replacement mechanism has been reported previously. The Kaapvaal polymict xenoliths provide evidence of metasomatic transformation of clinopyroxene to orthopyroxene at temperatures and pressures within the garnet stability field of the lower lithosphere in the presence of kimberlitic-carbonatitic melts. The protolith to the polymict

rock is believed to be predominantly lherzolite as indicated by the occurrence of garnets with lherzolitic affinities. The silica-rich metasomatism reported here may be the process required to explain the petrology of the lower lithosphere beneath cratons. Appropriate pathways for fluid ingress within the lower lithosphere are shear zones in high-temperature sheared garnet- and spinel-facies xenoliths (Cabanes and Briqueu, 1987; Witt and Seck, 1987; Smith et al., 1993; Zangana et al., 1997), which may be caused by crack propagation. Such cracks are sites of preferential deformation and melt percolation and as such, an integral part of the entrainment process.

Acknowledgments—This work represents part of the doctoral thesis work of H. Z, undertaken at Royal Holloway and funded by the Overseas Research Students Scheme (UK) and the K. C. Wong Education Foundation (Hong Kong) both of which are thanked for their financial support. We are grateful to A. Beard, R. Hinton, D. Mattey, N. Grassineau, and D. Lowry for their assistance with elemental and oxygen isotope analyses and to B. Ronald Frost for his editorial handling and his instruction with the P-T calculation and the QUILF program. Reviews of a much earlier version of this manuscript by B. Ronald Frost, Peter Kelemen, and two anonymous reviewers are greatly appreciated. Their thorough, and in most cases, constructive reviews resulted in substantial improvements to the paper. Funds from the Chinese National Science Foundation (40073004) and Chinese Academy of Sciences (KZCX1 to 07) are also gratefully acknowledged.

Associate editor: B. R. Frost

REFERENCES

Anders E. and Grevesse N. (1989) Abundances of the elements: Meteoritic and solar. *Geochim. Cosmochim. Acta* **53,** 197–214.

Andersen D. J., Lindsley D. H., and Davidson P. M. (1993) QUILF: A Pascal program to assess equilibria among Fe-Mg-Mn-Ti oxides, pyroxenes, olivine, and quartz. *Comput. Geosci.* **19,** 1333–1350.

Boyd F. R. (1989) Compositional distinction between oceanic and cratonic lithosphere. *Earth Planet. Sci. Lett.* **96,** 15–26.

Boyd F. R. and Canil D. (1997) *Peridotite xenoliths from the Slave craton, Northwest Territories.* Seventh Annual V. M. Goldschmidt Conference, Arizona, pp. 34–35.

Boyd F. R. and Nixon P. H. (1978) Ultramafic nodules from the Kimberley pipes, South Africa. *Geochim. Cosmochim. Acta* **42,** 1367–1382.

Boyd F. R. Gurney J. J., and Richardson S. H. (1985) Evidence for a 150–200 km thick Archaean lithosphere from diamond inclusion thermobarometry. *Nature* **315,** 387–9.

Boyd F. R., Pearson D. G., Nixon P. H., and Mertzman S. A. (1993) Low-calcium garnet harzburgites from South Africa: Their relations to craton structure and diamond crystallization. *Contrib. Mineral. Petrol.* **113,** 352–366.

Boyd F. R., Pokhilenko N. P., Pearson D. G., Mertzman S. A., Sobolev N. V., and Finger L. W. (1997) Composition of the Siberian cratonic mantle: Evidence from Udachnaya peridotite xenoliths. *Contrib. Mineral. Petrol.* **128,** 228–246.

Brey G. P. and Köhler T. (1990) Geothermobarometry in four-phase lherzolites II. New thermobarometers, and practical assessment of existing thermobarometers. *J. Petrol.* **31,** 1353–1378.

Cabanes N. and Briqueu L. (1987) Hydration of an active shear zone: Interactions between deformation, metasomatism and magmatism-the spinel-lherzolites from the Montferrier (southern France) Oligocene basalts. *Earth Planet. Sci. Lett.* **81,** 233–244.

Canil D. (1992) Orthopyroxene stability along the peridotite solidus and the origin of cratonic lithosphere beneath southern Africa. *Earth Planet. Sci. Lett.* **111,** 83–95.

Carswell D. A. and Dawson J. B. (1970) Garnet peridotite xenoliths in South Africa kimberlite pipes and their petrogenesis. *Contrib. Mineral. Petrol.* **25,** 163–184.

Chazot G., Lowry D., Menzies M. A., and Mattey D. P. (1997) Oxygen isotope composition of hydrous and anhydrous mantle peridotites. *Geochim. Cosmochim. Acta* **61,** 161–169.

Chen J. (1971) Petrology and chemistry of garnet lherzolite nodules in kimberlite from South Africa. *Am. Mineral.* **56,** 2098–2110.

Dawson J. B. (1990) *Kimberlites and Their Xenoliths.* Springer Verlag, Berlin, pp. 252.

Dawson J. B. (1987) Metasomatized harzburgites in kimberlite and alkaline magmas: Enriched restites and "flushed' lherzolites. In *Mantle Metasomatism* (ed. M. A. Menzies and C. J. Hawkesworth), Academic Press, London, pp. 125–144.

Eggins S. M., Rudnick R. L., and McDonough W. F. (1998) The composition of peridotites and their minerals: A laser-ablation ICP-MS study. *Earth Planet. Sci. Lett.* **154,** 53–71.

Ehrenberg S. N. (1982) Rare earth elements geochemistry of garnet lherzolite and megacrystalline nodules from minette of the Colorado plateau province. *Earth Planet. Sci. Lett.* **57,** 191–210.

Erlank A. J., Waters F. G., Hawkesworth C. J., Haggerty S. E., Allsopp H. L., Rickard R. S., and Menzies M. A. (1987) Evidence for mantle metasomatism in peridotite nodules from Kimberley pipes, South Africa. In *Mantle Metasomatism* (ed. M. A. Menzies and C. J. Hawkesworth), Academic Press, pp. 221–309.

Finnerty A. A. and Boyd F. R. (1987) Thermobarometry for garnet peridotites: Basis for the determination of thermal and compositional structure of the upper mantle. In *Mantle Xenoliths* (ed. P. H. Nixon), John Wiley & Sons, pp. 381–402.

Foley S. F., Jenner S. E., and Fryer B. J. (1994) Trace element partition coefficients between phlogopite, clinopyroxene and matrix in an alkaline lamprophyre from Newfoundland, Canada. *Mineral. Mag.* **58A,** 280–281.

Frost B. R. and Lindsley D. H. (1992) Equilibria among Fe-Ti oxides, pyroxenes, olivine, and quartz: Part II. Application. *Am. Mineral.* **77,** 1004–1020.

Griffin W. L., Shee S. R., Ryan C. G., Win T. T., and Wyatt B. A. (1999) Harzburgite to lherzolite and back again: Metasomatic processes in ultramafic xenoliths from the Wesselton kimberlite, Kimberley, South Africa. *Contrib. Mineral. Petrol.* **134,** 232–250.

Haggerty S. E. (1989a) Upper mantle opaque mineral stratigraphy and the genesis of metasomites and alkali-rich melts. *J. Geol. Soc. Aust., Special Publication* **14,** 687–699.

Haggerty S. E. (1989b) Mantle metasomes and the kinship between carbonatites and kimberlites. In *Carbonatite-Genesis and Evolution* (ed. K. Bell), Allen and Unwin, London, pp. 546–560.

Hanson G. N. and Langmuir C. H. (1978) Modeling of major elements in mantle-melt systems using trace element approaches. *Geochim. Cosmochim. Acta* **42,** 725–741.

Harte H., Winterburn P. A., and Gurney J. J. (1987) Metasomatic and enrichment phenomena in garnet peridotite facies mantle xenoliths from the Matsoku kimberlite pipe, Lesotho. In *Mantle Metasomatism* (ed. M. A. Menzies and C. J. Hawkesworth), Academic Press, pp. 145–220.

Harte B. and Kirkley M. B. (1997) Partitioning of trace elements between clinopyroxene and garnet:data from mantle eclogites. *Chem. Geol.* **136,** 1–24.

Herzberg C. T. (1993) Lithosphere peridotites of the Kaapvaal craton. *Earth Planet. Sci. Lett.* **120,** 13–29.

Herzberg C. T. (1999) Phase equilibrium constraints on the formation of cratonic mantle. In *Mantle Petrology: Field Observations and High Pressure Experiments* (ed. Y. Fei, C. M. Berthka, and B. O. Mysen), Spec. Pub. Geochem. Soc. No. 6, pp. 241–257.

Johnson K. T. M. (1998) Experimental determination of partition coefficients for rare earth and high-field-strength elements between clinopyroxene, garnet, and basaltic melt at high pressures. *Contrib. Mineral. Petrol.* **133,** 60–68.

Jones J. H. and McKay G. A. (1992) REE partitioning between pyroxene liquid and garnet/liquid parameterization using DCa. *EOS T. Am. Geophys. Un.* **73,** 607.

Jordan T. H. (1978) Composition and development of the continental tectosphere. *Nature* **274,** 544–548.

Kelemen P. B., Dick H. J. B., and Quick J. E. (1992) Formation of harzburgite by pervasive melt/rock reaction in the upper mantle. *Nature* **358,** 635–641.

Kelemen P. B., Hart S. R., and Bernstein S. (1998) Silica enrichment

in the continental upper mantle via melt/rock reaction. *Earth Planet. Sci. Lett.* **164,** 387–406.

Kelemen P. B., Johnson K. T. M., Kinzler R. J., and Irving A. J. (1990) High-field-strength element depletions in arc basalts due to mantle-magma interaction. *Nature* **345,** 521–524.

Kelemen P. B., Shimizu N., and Dunn T. (1993) Relative depletion of niobium in some arc magmas and the continental crust: Partitioning of K, Nb, La and Ce during melt/rock reaction in upper mantle. *Earth Planet. Sci. Lett.* **120,** 111–134.

Kramers J. D., Roddick J. C. M., and Dawson J. B. (1983) Trace element and isotope studies on veined, metasomatic and "MARID" xenoliths from Bultfontein, Southern Africa. *Earth Planet. Sci. Lett.* **65,** 90–106.

Lawless P. J., Gurney J. J., and Dawson J. B. (1979) Polymict peridotites from the Bultfontein and De Beers mines, Kimberley, South Africa. *The mantle sample: Inclusions in kimberlites and other volcanics. Proceedings of Sec. Int. Kimb. Conf.* **2,** 145–155.

Lowry D., Mattey D. P., Macpherson C. G., and Harris J. W. (1993) Oxygen isotope variations among peridotitic and eclogitic syngenetic inclusions in diamond. *Terra Abstracts* **5,** 375.

Lowry D., Mattey D. P., Macpherson C. G., and Harris J. W. (1994) Evidence for stable isotope and chemical disequilibrium associated with diamond formation in the mantle. *Mineral. Mag.* **58A,** 535–536.

Maaloe S. and Aoki K. (1977) The major element composition of the upper mantle estimated from the composition of lherzolites. *Contrib. Mineral. Petrol.* **63,** 161–173.

MacKenzie J. M. and Canil D. (1999) Composition and thermal evolution of cratonic mantle beneath the central Archaean Slave Province, NWT, Canada. *Contrib. Mineral. Petrol.* **134,** 313–324.

Mathias M., Siebert J. C., and Rickwood P. C. (1970) Some aspects of the mineralogy and petrology of ultramafic xenoliths in kimberlite. *Contrib. Mineral. Petrol.* **26,** 75–123.

Mattey D. P., Lowry D., and Macpherson C. G. (1994a) Oxygen isotope composition of mantle. *Earth Planet. Sci. Lett.* **128,** 231–241.

Mattey D. P., Lowry D., Macpherson C. G., and Chazot G. (1994b) Oxygen isotope composition of mantle minerals by laser fluorination analysis: Homogeneity in peridotites, heterogeneity in eclogites. *Mineral. Mag.* **58A,** 573–574.

Menzies M. A., Rogers N., Tindle A., and Hawkesworth C. J. (1987) Metasomatic and enrichment processes in lithospheric peridotites, an effect of asthenosphere-lithosphere interaction. In *Mantle Metasomatism* (ed. M. A. Menzies and C. J. Hawkesworth), Academic Press, pp. 313–359.

Meyer H. O. A. (1987) Inclusions in diamond. In *Mantle Xenoliths* (ed. P. H. Nixon), John Wiley & Sons, pp. 501–522.

Morfi L., Harte B., Hill P., and Gurney J. (1999a) Polymict peridotites a link between deformed peridotites and megacrysts from kimberlites. *Ofioliti* **24,** 134.

Morfi L., Harte B., Hill P., and Gurney J. (1999b) Spatial relationships of compositional variation of polymict peridotites from kimberlites. *Ofioliti* **24,** 135–136.

Mitchell R. H. (1986) *Kimberlites: Mineralogy, Geochemistry, and Petrology.* Plenum Press, London, pp. 442.

Muramatsu Y. (1983) Geochemical investigation of kimberlites from the Kimberley area, South Africa. *Geochem. J.* **17,** 71–86.

Nelson D. R., Chivas A. R., Chappell B. W., and McCulloch M. T. (1988) Geochemical and isotopic systematics in carbonatites and implications for the evolution of ocean-island sources. *Geochim. Cosmochim. Acta* **52,** 1–17.

Nixon P. H. (1987) Kimberlitic xenoliths and their cratonic setting. In *Mantle Xenoliths* (ed. P. H. Nixon) John Wiley & Sons, pp. 215–239.

Nixon P. H. and Boyd F. R. (1973) Petrogenesis of the granular and sheared ultrabasic nodule suite in kimberlites. In *Lesotho Kimberlites* (ed. P. H. Nixon), Lesotho National Development Corporation, pp. 48–56.

Olive V., Ellam R. M., and Harte B. (1997) A Re-Os isotope study of ultramafic xenoliths from the Matsoku kimberlite. *Earth Planet. Sci. Lett.* **150,** 129–140.

Quick J. E. (1981) The origin and significance of large tabular dunite bodies in the Trinity peridotite, northern California. *Contrib. Mineral. Petrol.* **78,** 413–422.

Ringwood A. E. (1958) The constitution of the mantle-III: Consequences of the olivine-spinel transition. *Geochim. Cosmochim. Acta* **15,** 195–212.

Rudnick R. L., McDonough W. F., and Orpin A. (1994) Northern Tanzanian peridotite xenoliths: A comparison with Kaapvaal peridotites and inferences on metasomatic interactions. In *Kimberlites, Related Rocks and Mantle Xenoliths* (ed. H. O. A. Meyer and O. Leonardos), Vol. 1, pp. 336–353, Proceedings Fifth Int. Kimb. Conf., CPRM.

Schwandt C. S. and McKay G. A. (1998) Rare earth element partion coefficients from enstatite/melt synthesis experiments. *Geochim. Cosmochim. Acta* **62,** 2845–2848.

Schulze D. J. (1991) Low-Ca garnet harzburgite xenoliths from southern Africa: Abundance, composition, and bearing on the structure and evolution of the subcratonic lithosphere. Ext. Abstr. 5th Int. Kimb. Conf., Araxa, Brazil. CPRM special publication **2/91,** 350–352.

Smith D., Griffin W. L., and Ryan C. G. (1993) Compositional evolution of high-temperature sheared lherzolite PHN1611. *Geochim. Cosmochim. Acta* **57,** 605–613.

Waters F. G. (1987) *A Geochemical Study of Metasomatized Peridotite and MARID Nodules from the Kimberley Pipes, South Africa.* Unpubl. Ph.D. thesis, University of Cape Town.

Walker R. J., Carlson R. W., Shirey S. B., and Boyd, F. R. (1989) Os, Sr, Nd, and Pb isotope systematics of southern African peridotites xenoliths: Implications for the chemical evolution of subcontinental mantle. *Geochim. Cosmochim. Acta* **53,** 1583–1595.

Walter M. J. (1998) Melting of garnet peridotite and the origin of komatiite and depleted lithosphere. *J. Petrol.* **39,** 29–60.

Walter, M. J. (1999) Melting residue of fertile peridotite and the origin of cratonic lithosphere. In *Mantle Petrology: Field Observations and High Pressure Experiments* (ed. Y. Fei, C. M. Berthka, and B. O. Mysen), Spec. Pub. Geochem. Soc. No. 6, pp. 225–239.

Witt G. E. and Seck H. A. (1987) Temperature history of sheared mantle xenoliths from the west Eifel, West Germany: Evidence for mantle diapirism beneath the Rhenish Massif. *J. Petrol.* **28,** 75–493.

Woolley A. R. and Kempe D. R. C. (1989) Carbonatites: Nomenclature, average chemical compositions, and element distribution. In *Carbonates Genesis and Evolution* (ed. K. Bell), Allen and Unwin, London, pp. 1–14.

Xu Y. -G., Menzies M. A., Mattey D. P., Lowry D., Harte B., and Hinton R. W. (1996) The nature of the lithospheric mantle near the Tancheng-Lujiang fault, China: An integration of texture, chemistry and O-isotopes. *Chem. Geol.* **134,** 67–81.

Zangana N. A., Downes H., Thirlwall M. F., and Hegner E. (1997) Relationship between deformation, equilibration temperatures, REE and radiogenic isotopes in mantle xenoliths (Ray Pic, Massif Central, France): An example of plume-lithosphere interaction? *Contrib. Mineral. Petrol.* **127,** 187–203.

Zhang H. -F. (1998) *Petrology and Geochemistry of On- and Off-Craton Mantle Rocks: Eastern China and Southern Africa.* Ph.D. thesis, Royal Holloway, University of London.

Zhang H. -F., Mattey D. P., Grassineau N., Lowry D., Brownless M. Gurney J. J., and Menzies M. A. (2000). Recent fluid processes in the Kaapvaal craton, South Africa: Coupled oxygen isotope and trace element disequilibrium in polymict peridotites. *Earth Planet. Sci. Lett.* **57,** 57–72.